

UCRL-JC-132104

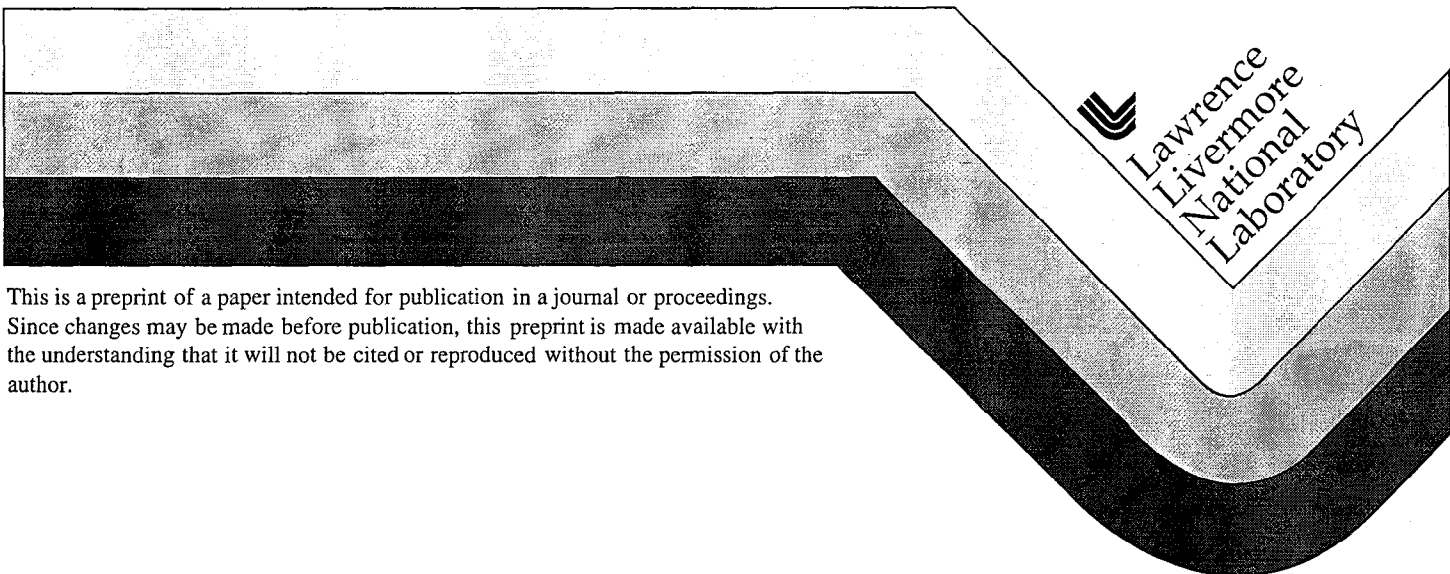
PREPRINT

Superconducting Tunnel Junction Array Development for High-Resolution Energy-Dispersive X-Ray Spectroscopy

S. Friedrich, C. A. Mears, B. Nideröst, L. J. Hiller, M. Frank,
S. E. Labov, A. T. Barfknecht, S. P. Cramer

This paper was prepared for submittal to
1998 Microscopy and Microanalysis Conference
Atlanta, GA
July 12-16, 1998

July 1, 1998



This is a preprint of a paper intended for publication in a journal or proceedings.
Since changes may be made before publication, this preprint is made available with
the understanding that it will not be cited or reproduced without the permission of the
author.

DISCLAIMER

This document was prepared as an account of work sponsored by an agency of the United States Government. Neither the United States Government nor the University of California nor any of their employees, makes any warranty, express or implied, or assumes any legal liability or responsibility for the accuracy, completeness, or usefulness of any information, apparatus, product, or process disclosed, or represents that its use would not infringe privately owned rights. Reference herein to any specific commercial product, process, or service by trade name, trademark, manufacturer, or otherwise, does not necessarily constitute or imply its endorsement, recommendation, or favoring by the United States Government or the University of California. The views and opinions of authors expressed herein do not necessarily state or reflect those of the United States Government or the University of California, and shall not be used for advertising or product endorsement purposes.

Superconducting Tunnel Junction Array Development
for High-Resolution Energy-Dispersive X-Ray Spectroscopy

S. Friedrich^{a,c,*}, C.A. Mears^a, B. Nideröst^a, L.J. Hiller^a, M. Frank^a,
S.E. Labov^a, A.T. Barfknecht^b, S.P. Cramer^c

(a) Lawrence Livermore National Lab, P.O. Box 808, L-418, Livermore, CA 94550, USA

(b) Conductus Inc., 969 West Maude Ave., Sunnyvale, CA 94086, USA

(c) Lawrence Berkeley National Lab, MS 6-2100, Berkeley, CA 94720, USA

Abstract

Cryogenic energy-dispersive x-ray detectors are being developed because of their superior energy resolution (≤ 10 eV FWHM for keV x rays) compared to semiconductor EDS systems. So far, their range of application is limited due to their comparably small size and low count rate. We present data on the development of superconducting tunnel junction (STJ) detector *arrays* to address both of these issues. A single STJ detector has a resolution around 10 eV below 1 keV and can be operated at count rates of order 10,000 counts/s. We show that the simultaneous operation of several STJ detectors does not diminish their energy resolution significantly, while increasing the detector area and the maximum count rate by a factor given by the total number of independent channels.

Keywords: Cryogenic x-ray detectors; superconducting tunnel junctions; x-ray microcalorimeter; detector arrays

*Corresponding author; friedrich1@llnl.gov

Introduction

Over the last 10 years, there has been an increasing interest in energy-dispersive x-ray detectors operated at temperatures below 1 K, which offer energy resolution comparable to wavelength-dispersive spectrometers [1, 2]. The detector development was initially driven by x-ray and particle astrophysics [3,4]. More recently, applications in microanalysis [5], material science [6] and biophysics [7, 8] have emerged and are being pursued for scientific and commercial interest.

Cryogenic x-ray detectors fall into two groups: Microcalorimeters and superconducting tunnel junctions (STJs). Microcalorimeters measure the x-ray induced temperature rise of a sensitive thermistor, typically a doped semiconductor [4, 9] or a superconducting transition edge sensor [5]. Microcalorimeters offer a very high energy resolution below 8 eV FWHM at 6 keV [4, 5, 9]. This comes at the expense of a lower maximum count rate around 500 counts/s, because the relaxation of thermal devices back to their equilibrium is intrinsically slow [5]. STJ detectors offer a slightly poorer resolution of 15.7 eV FWHM at 6 keV [10], unless future devices employ superconductors with extremely low critical temperatures [11, 12, 13]. However, STJ detectors can be operated at significantly higher count rates of order 10,000 counts/s [14].

One common challenge with cryogenic x-ray detectors is their comparably small size, typically of order $200 \times 200 \mu\text{m}^2$. Simply increasing device size tends to degrade the resolution because of added heat capacity (for microcalorimeters) or capacitance (for STJs) or because of spatially varying detector response. Several approaches are being pursued to increase the effective detector area. One of them is to separate absorber and detector function and couple a large absorber with a small detector [3, 15, 16]. This slows down the detector response and can complicate the spectral analysis. Another approach is to use polycapillary focusing optics [5] to increase the effective solid angle. This is at present rather costly and may exceed the detector's maximum count rate capability.

Here we report on the development of STJ detector arrays. Arrays not only increase the detector area, but also the maximum count rate by a factor given by the total number of independent channels. The complexity and cost of operating a multi-channel array is acceptable in microanalysis and material science applications for arrays with of order 10 independent channels. Further increases of detector efficiency are then more likely to be obtained by using an x-ray focusing optics.

STJ Operating Principle

Superconducting tunnel junctions (STJs) consist of two superconducting electrodes separated by a thin insulator. They use the small energy gap by which excited single-

particle states (so-called quasiparticles) are separated from the Cooper pairs that constitute the superconducting electronic ground state. An x-ray photon absorbed in one of the electrodes breaks Cooper pairs and thereby generates excess quasiparticles in proportion to its energy. The quasiparticles can tunnel through the insulating barrier and thereby produce an increased current proportional to the energy of the incoming x-ray. STJ detectors rely on measuring the excess current after x-ray absorption. As such, their operating principle is similar to that of conventional semiconductor Si(Li) or Ge detectors. One essential difference is that the gap in superconductors is of order 1 meV, about a factor 1000 smaller compared to the gap in semiconductors. X-rays therefore generate roughly 1000 times more excess charge carriers in superconductors compared to semiconductors. Theoretically, this results in an improved theoretical energy resolution by a factor $\sqrt{1000} \approx 30$. For Nb-based STJs, the statistics of the initial charge generation ultimately limit the resolution to values between 0.8 and 1.7 eV FWHM for x-ray energies between 0.2 and 1 keV [13]. In most practical devices, additional fluctuations in the number of tunneling events reduce the theoretically attainable resolution in that energy range by a factor ≈ 2.5 [17].

Detector efficiency can be increased through a process called quasiparticle trapping [3, 18]. It employs an absorber with a large energy gap in connection with a tunnel junction made from a smaller gap superconductor. Quasiparticles which have diffused from the large gap absorber into the lower gap material relax energetically by phonon emission and are then "trapped" in the potential well close to the tunneling barrier. Trapping separates the absorber from the detector function in the device. The absorber film can be made thick and from a high Z material for high efficiency, while the trapping layer can be made thin for fast tunneling. Trapping also increases the life time of the quasiparticles, as it keeps them away from the possibly degraded detector surface. If a large gap superconductor is used on either side of the tunnel junction, the quasiparticles will remain in the lower gap junction region until they recombine and form Cooper pairs again. These processes cause the current waveform from an STJ detector to exhibit a fast rise corresponding to fast quasiparticle diffusion to the tunnel barrier and a slower exponential decay with a time constant set by quasiparticle recombination. A cross sectional drawing of our STJ detectors is shown in figure 1.

The quasiparticle recombination time in the junction electrodes also determines the maximum count rate of STJ detectors. Ideally, quasiparticles from a previous absorption event should have relaxed to their ground state before the STJ detector measures another x-ray. Otherwise, pile-up will start to reduce the detector performance. Typical recombination times in our superconducting detectors are of order 2 - 10 μ s [figure 2]. This allows STJ

detector operation at count rates of several 1000 counts/s with undiminished energy resolution. Operation at higher rates is possible with somewhat lower resolution due to pile-up [14].

Experimental Results

We are developing STJ spectrometers based on Nb-Al-AlO_x-Al-Nb thin film technology. In earlier experiments, our small $50 \times 50 \mu\text{m}^2$ devices have shown an energy resolution between 4.6 and 8.9 eV FWHM for x-ray energies between 0.2 and 1 keV [12]. The device discussed here is a linear array of four $200 \times 200 \mu\text{m}^2$ STJ detectors. Each detector consists of a separate 265 nm bottom Nb film, an Al-AlO_x-Al tunnel junction with 50 thick Al electrodes, and a 165 nm top Nb absorber. The devices are fabricated at Conductus Inc. in Sunnyvale, CA, using a modified photolithographic trilayer process [19]. Details of the fabrication process have been published elsewhere [17].

The STJ detectors are operated in a liquid helium cryostat with an adiabatic demagnetization refrigerator (ADR) stage. It attains a base temperature of 60 mK and can easily be attached to a synchrotron beam line. The ADR has a hold time of 4 – 6 hours below 0.4 K and requires about 30 minutes to cycle. Note that the temperature does not need to be regulated for the operation of these devices as long as it remains below 0.4 K. We apply a magnetic field of ≈ 100 Gauss parallel to the device in direction of the junction diagonal to suppress the dc Josephson current and reduce the magnitude of Fiske mode resonances [20]. This is required for bias stability at the operating voltage of $\approx 400 \mu\text{V}$. For fluorescence experiments, we insert a sample stage through a load lock to within 5 mm of the STJ detector. A single $200 \times 200 \mu\text{m}^2$ detector then covers a solid angle of $1.6 \cdot 10^{-3}$ sr. This small device size necessitates placing the sample close to the detector (and thus at cryogenic temperatures) and motivates the development of STJ arrays. Fortunately, photolithographic device fabrication and a preamplifier with an off-the-shelf FET input stage allow easy scaling to multi-element arrays. For details of the experimental setup see [6].

One concern for the operation of detector arrays is device uniformity. Our experience with photolithographically fabricated devices over the last five years has been that when a wafer contains high quality junctions, then all devices on that wafer tend to be good. The dc device $I(V)$ characteristics tend to be very similar, although not identical. This is important because the same magnetic field must be used to suppress the dc Josephson current and the Fiske mode resonances in all STJ devices of the array [21]. We found that it was not difficult to achieve the necessary suppression simultaneously for all the detectors in the array. Furthermore, future preamplifiers will employ dc voltage biasing rather than

biasing at a constant dc current to further reduce the influence of Fiske mode resonances on device operation [16].

Figure 3 shows two fluorescence spectra of a hydrogenase sample, an enzyme from the bacterium *Desulfovibrio gigas* that is responsible for hydrogen evolution and uptake [22]. The spectra were acquired simultaneously with two neighboring $200 \times 200 \mu\text{m}^2$ detectors of a linear four element array. Each of the detectors had its own electrical ground and electronic readout. Both detectors show nearly identical spectral response, differing only in an overall gain factor which has been corrected for by the calibration procedure used to convert the pulse height to x-ray energy. The two prominent peaks at 277 eV and 525 eV are K-shell x-rays from the carbon and oxygen that make up the bulk of the enzyme. The small peaks to the right of the oxygen line are the iron L_{α} and nickel L_{α} lines. The sample contains about 500 ppm Ni and 12 times more Fe. The number of counts in the Fe and the Ni lines do not reflect the 12:1 abundance ratio of Fe to Ni, because Fe is excited less efficiently by the incident radiation, and because residual gases frozen out on the sample attenuate the Fe signal more strongly than the higher-energy Ni fluorescence. The double peak structure above 900 eV is mostly due to scatter of the incident 970 eV x-ray beam, with a small shoulder on the low energy side from the nickel $L_{\beta_{3,4}}$ line. The peak at 1041 eV is due to sodium used in sample preparation which is excited by the second order radiation of the synchrotron beam.

The resolution of the two devices individually is 10.7 and 10.9 eV FWHM at carbon K and 12.6 and 12.8 eV at oxygen K, respectively. There is an uncertainty of ± 0.2 eV in the resolution because of ambiguities in how to subtract the spectral background at the different fluorescence lines. No electronic pulses were injected during this particular run to measure the contribution of the readout electronics to the line width. However, spectra taken earlier under identical conditions with the same device had an electronic noise contribution around 9 eV. The response of the two devices is sufficiently similar to allow adding the two spectra. The combined spectrum of the two channels has a resolution of 10.9 eV at carbon K (277 eV) and 12.9 eV at oxygen K (525 eV), respectively. Adding the two spectra broadens the lines only marginally. This makes us confident that scaling to larger arrays can be accomplished without much further loss in resolution.

While the detector resolution of the $200 \times 200 \mu\text{m}^2$ devices is poorer than the resolution of smaller devices [12], is still sufficient to fully separate the Ni L and the Fe L fluorescence from the strong oxygen K line centered at 525 eV. In many applications, it is desirable to trade off resolution for larger solid angle coverage as long as the detector can handle the higher count rate. This is particularly important for the fast analysis of dilute

samples, where a sufficiently high number of counts in the weak signal line is accompanied by a huge number of counts from other elements in the sample. For example, the metalloprotein spectra shown in figure 3 contain a total of $\approx 310,000$ counts just in the oxygen K line, compared to ≈ 3200 counts in the Ni L_{α} line.

Crosstalk is another concern for operating multi-element arrays. The question whether an event in one of the detector elements will induce a signal in the neighboring detectors is particularly important when the two detectors are located immediately next to each other, as would be desirable in a detector array to be used with a focusing optics. We have measured the level of crosstalk between neighboring devices by triggering on events from only one channel and plotting the response of both channels averaged over 1000 individual events [figure 2]. The signal in channel 1 is mostly due to carbon and oxygen K fluorescence photons as seen in the spectra [figure 3]. The waveform shows the fast rise time, limited by the response of the preamplifier, followed by an exponential decay with a time constant characteristic for the lifetime of the excess quasiparticles in the aluminum layers of the tunnel junction. The small correlated bipolar signal in channel 2 is the only evidence of crosstalk we observe. It is magnified by a factor 10 for clarity and it is not detectable at all without averaging. The amplitude of the signal in channel 2 is less than 0.1% of the peak-to-peak signal in channel 1. Because of its short duration and bipolar nature, crosstalk effects are even further removed by the low-pass filtering procedure we typically use to reduce the effects of high-frequency noise. Crosstalk therefore does not limit the operation of our STJ detector arrays.

Future devices will replace the niobium with tantalum for better absorption efficiency at higher x-ray energies. We are also planning to build a 3×3 STJ array spectrometer [inset figure 1], coupled with an x-ray focusing optics which offers a resolution below 10 eV at energies up to 1 keV and a total count rate well above 100,000 counts/s. It will cover a solid angle of 0.1 sr and will have a quantum efficiency between 10 and 20% depending on the particular type of optics used.

Summary

We are developing Nb-based superconducting tunnel junctions (STJs) as high-resolution energy-dispersive x-ray spectrometers. Small $50 \times 50 \mu\text{m}^2$ have an energy resolution between 4.6 and 8.9 eV FWHM for x-ray energies between 0.2 and 1 keV and can be operated at count rates of order $\approx 10,000$ counts/s. Larger $200 \times 200 \mu\text{m}^2$ STJ detectors have somewhat poorer resolution, typically around 12 eV due to higher device capacitance. We have operated two $200 \times 200 \mu\text{m}^2$ devices from a multi-element array simultaneously without significant loss in detector resolution. A 3×3 detector array

currently being developed will have an active area of $0.6 \times 0.6 \text{ mm}^2$ and is expected to operate at total count rates above 100,000 counts/s.

Acknowledgments

We thank Jan Batteaux and Jeff Moore for expert technical assistance. This work was performed under the auspices of the U.S. Department of Energy by LLNL under contract No. W-7405-ENG-48 at the Stanford Synchrotron Radiation Laboratory (SSRL) which is operated by the DOE, Office of Basic Energy Sciences. Funding for this research was provided by the DOE, Office of Biological and Environmental Research, by the NIH through grant No. GM 44380, and by NASA through SBIR Contract No. NAS5-32805 and through UV detector development grant No. NAG5-4137.

References

1. N.E. Booth, D.J. Goldie, *Supercond. Sci. Technol.* **9**, 493 (1996)
2. D. Twerenbold, *Rep. Prog. Phys.* **59**, 349 (1996)
3. H. Kraus, F. v. Freilitzsch, J. Jochum, R.L. Mössbauer, T. Peterreins, F. Pröbst, *Phys. Lett.* **B231**, 195 (1989)
4. D. McCammon, W. Cui, M. Juda, J. Morgenthaler, J. Zhang, R. L. Kelley, S.S. Holt, G.M. Madejski, S.H. Moseley, A.E. Szymkowiak, *Nucl. Inst. Meth.* **A326**, 157 (1993)
5. D.A. Wollman, K.D. Irwin, G.C. Hilton, L.L. Dulcie, D.E. Newbury, J.M. Martinis, *J. Microscopy* **188**, 196 (1997)
6. M. Frank, C.A. Mears, S.E. Labov, L.J. Hiller, J.B. LeGrand, M.A. Lindeman, H. Netel, D. Chow, A.T. Barfknecht, *J. Synchrotron Rad.* **5**, 515 (1998)
7. W. H. Benner, D.M. Horn, J.M. Jaklevic, M. Frank, C.A. Mears, S.E. Labov, A.T. Barfknecht, *J. Am. Soc. Mass Spectrom.* **8**, 1094 (1997)
8. S. Friedrich, L.J. Hiller, M. Frank, J.B. le Grand, C.A. Mears, B. Nideröst, S.E. Labov, A.T. Barfknecht, M. LeGros, S.P. Cramer, accepted for publication in *J. of Electron Spectroscopy and Related Phenomena* (1999)
9. E. Silver, M. LeGros, N. Madden, J. Beeman, E. Haller, *X-Ray Spectrometry* **25**, 115 (1996).
10. P. Verhoeve, N. Rando, A. Peacock, A. van Dordrecht, B.G. Taylor, D.J. Goldie, *Appl. Phys. Lett.* **72**, 3359 (1998)

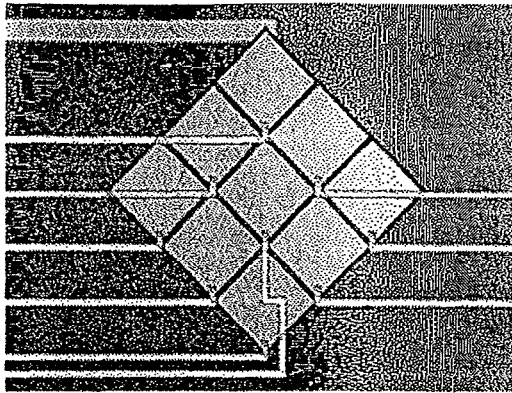
11. A. Peacock, P. Verhoeve, N. Rando, A. van Dordrecht, B.G. Taylor, C. Erd, M.A.C. Perryman, R. Venn, J. Howlett, D.J. Goldie, L. Lumley, M. Wallis, *Nature* **381**, 135 (1996)
12. J.B. LeGrand, C.A. Mears, L.J. Hiller, M. Frank, S.E. Labov, H. Netel, D. Chow, S. Friedrich, M.A. Lindeman, A.T. Barfknecht, *Appl. Phys. Lett.* **73** (1998), in press.
13. S. Kraft, A. Peacock, M. Bavdaz, B. Castello, B. Collaudin, D. Perez, R. Venn, *SPIE Proceedings* **3445** (1998)
14. M. Frank, L.J. Hiller, J.B. LeGrand, C.A. Mears, S.E. Labov, M.A. Lindeman, H. Netel, D. Chow, A.T. Barfknecht, *Rev. Sci. Inst.* **69**, 25 (1998)
15. P. Ferger et al., *Nucl. Inst. Meth.* **A370**, 157 (1996)
16. S. Friedrich, K. Segall, M.C. Gaidis, C.M. Wilson, D.E. Prober, P.J. Kindlmann, A.E. Szymkowiak, S.H. Moseley, *IEEE Trans. Appl. Supercon.* **7**, 3383 (1997)
17. C.A. Mears, S.E. Labov, A.T. Barfknecht, *Appl. Phys. Lett.* **63**, 2961 (1993)
18. N.E. Booth, *Appl. Phys. Lett.* **50**, 293 (1987)
19. A.T. Barfknecht, R.C. Ruby, H. Ko, *IEEE Trans. Magn.* **27**, 970 (1991)
20. M.D. Fiske, *Rev. Mod. Phys.* **36**, 221 (1964)
21. R. den Hartog, A. Peacock, P. Verhoeve, F. Jansen, J. Verveer, A. van Dordrecht, J. Salmi, R. Venn, *SPIE Proceedings* **3114**, 310 (1997)
22. "The Bioinorganic Chemistry of Nickel", J.R. Lancaster ed., VCH Publishers (1988)

Figure Captions

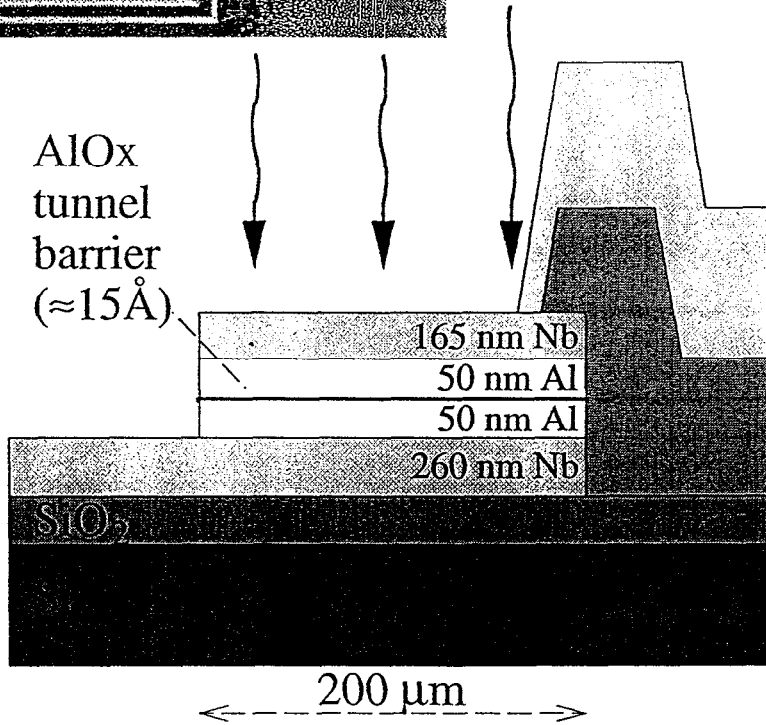
Figure 1: Cross section of an STJ detector. An x ray breaks Cooper pairs in the top Nb absorber thereby generating free excess charges which scatter into the Al trap and produce a current pulse as they tunnel through the AlOx barrier. The inset shows a 3×3 array of $200 \times 200 \mu\text{m}^2$ STJ detectors currently being developed.

Figure 2: Average waveform of 1000 events, mostly C K and O K fluorescence. The trigger was set to channel 1, and the signal induced in channel 2 due to crosstalk is negligibly small. Channel 2 is magnified by a factor 10 for clarity.

Figure 3: Fluorescence spectrum of the metalloprotein Hydrogenase (≈ 500 ppm Ni) using two STJ detectors of a linear array. Both devices show a very similar spectral response. The excitation energy was 970 eV.



X-Rays



AlO_x
tunnel
barrier
(≈15Å)

165 nm Nb
50 nm Al
50 nm Al
260 nm Nb

SiO₂

200 μm

